PHYSICAL REVIEW E **76**, 010501(R) (2007)

Simulations of dynamics and viscoelasticity in highly entangled solutions of semiflexible rods

Shriram Ramanathan and David C. Morse*

Department of Chemical Engineering and Materials Science, University of Minnesota, Minneapolis, Minnesota 55455, USA

(Received 22 January 2007; published 6 July 2007)

Brownian dynamics simulations are used to study highly entangled solutions of semiflexible polymers. Bending fluctuations of semiflexible rods are significantly affected by entanglement only above a concentration c^{**}, where $c^{**} \sim 10^3 L^{-3}$ for chains of length L similar to their persistence length. For $c > c^{**}$, the tube radius R_e approaches a dependence $R_e \propto c^{-3/5}$ and the linear viscoelastic response develops an elastic plateau that is absent for $c < c^{**}$. Experiments on isotropic solutions of F-actin are shown to span concentrations near c^{**} for which the predicted asymptotic scaling of the plateau modulus, $G \propto c^{7/5}$, is not yet valid.

DOI: 10.1103/PhysRevE.76.010501 PACS number(s): 83.10.Mj, 83.80.Tc, 87.15.Aa

Solutions of long polymers become entangled when the concentration or chain length exceeds a threshhold. The nature of "entanglement" is obviously different, however, for random walks, rigid rods, and semiflexible threads. It has been proposed that solutions of semiflexible rods, of length L less than or equal to their persistence length L_p, may exhibit two different levels of entanglement, in different concentration regimes [1–7]—a loosely entangled regime, in which only rotations and transverse translations are hindered by collisions, and a tightly entangled regime, in which transverse bending fluctuations are also strongly affected. The crossover between these two regimes is expected to lead to a qualitative change in viscoelastic properties, due to the much slower relaxation in a tightly entangled solution of stress caused by transverse chain deformation. Clear experimental evidence of "tight" entanglement has been obtained only for solutions of very long actin protein filaments (F-actin), of length $L \sim L_p \sim 10$ μm and diameter $d \sim 10$ nm. The evidence comes both from visualization of flourescently labeled chains [8,9] and from rheological measurements [7,10–12]. It remains unclear, however, whether bending fluctuations are ever significantly hindered in isotropic solutions of any of a variety of other well-studied model systems of semiflexible rods with $L \sim L_p$ [13], for which the average chain lengths and aspect ratios are all much smaller than those obtainable with F-actin. Simulations offer a potentially important complement to the experimental study of these systems.

Consider a solution of thin semiflexible rods, each of contour length L and persistence length L_p, with $L \lesssim L_p$. Let c be the number density and $\rho \equiv cL$ be the contour length per volume. Simple geometrical arguments suggest the following sequence of concentration regimes [2,5]: At dilute concentrations $c < c^*$, where $c^* \propto L^{-3}$, chain motion is essentially unhindered. In the loosely entangled regime $c^* \ll c \ll c^{**}$, rotations and transverse rigid-body translations are strongly hindered, but transverse bending fluctuations are not. In this regime, each chain is trapped in a cylindrical cage or tube of radius $R_e \sim 1/(cL^2)$ [14]. Above a threshhold $c^{**} \sim \sqrt{L_p/L}c^*$, this cage becomes narrow enough to also hinder thermal bending fluctuations [1–3,5]. At concentrations $c \gg c^{**}$, chain motion can be described by a modified tube model [2,3] in which each chain undergoes reptation in a narrow wormlike tube. A scaling argument due to Odijk [1] and Semenov [3] predicts a tube radius $R_e \propto L_p(\rho L_p^2)^{-3/5}$ for $c \gg c^{**}$.

Our simulations use an algorithm that was designed to allow simulation of the Brownian motion of arbitrarily thin but uncrossable wormlike threads, which is discussed in detail elsewhere [15,16]. Each polymer is represented as a discretized chain of N inextensible rods and $N+1$ beads. At each step of the simulation, a trial move is generated for a randomly chosen chain by taking one time step of the Brownian dynamics (BD) algorithm that was used in our previous simulations of dilute solutions [17–19]. A trial move is rejected if it would cause the chosen chain to cut through any other. Here, we use an anisotropic local friction, with distinct longitudinal and transverse friction coefficients $\zeta_\parallel$ and $\zeta_\perp$ [19], with a ratio $\zeta_\parallel/\zeta_\perp = 1/2$ chosen to mimic the hydrodynamics of a slender filament. We present results here for chains with $L/L_p = 0.25$–2.0 and $N = 10$–40 rods at concentrations $cL^3 = 0$–4000. A 1-mg/ml solution of F-actin filaments with $L = 8$ μm would have $cL^3 \simeq 2500$.

To characterize the effect of entanglement upon bending fluctuations, we have calculated two measures of the transverse mean-squared displacement (MSD) of the middle bead of a polymer. The quantity $\langle \Delta d^2(t) \rangle$, shown in the main plot in Fig. 1, is the variance of the distance $\Delta d(t)$ between the middle bead at time t and the closest point on the contour of the same chain at an earlier time $t=0$. The inset instead shows $\langle \Delta \mathbf{r}_{m,\perp}^2(t) \rangle \equiv \langle |\mathbf{r}_{m,\perp}(t) - \mathbf{r}_{m,\perp}(0)|^2 \rangle$, in which $\mathbf{r}_{m,\perp}(t)$ is the transverse component (transverse to the local chain tangent) of the displacement of the middle bead from the chain's center of mass. The quantity $\langle \Delta \mathbf{r}_{m,\perp}^2(t) \rangle$ is not sensitive to center-of-mass diffusion, but only to displacements arising from bending fluctuations, and so approaches a finite value at long times. At early times, both of these quantities increase as $t^{3/4}$, as predicted [20]. With increasing concentration, both quantities become suppressed over a range of intermediate times, indicating the formation of a tube.

If each chain were confined to a tube of well-defined radius R_e over a wide range of intermediate times, $\langle \Delta d^2(t) \rangle$ would develop a plateau, with a plateau value $\langle \Delta d^2(t) \rangle \simeq 4R_e^2$. Here, R_e^2 is defined, as in Ref. [21], as the variance of the transverse displacement of the chain from the "center" of

*morse@cems.umn.edu

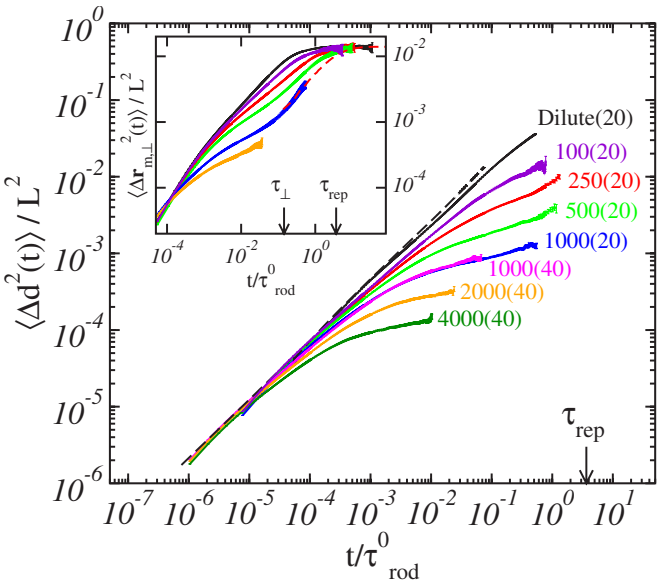

FIG. 1. (Color online) $\langle \Delta d^2(t)\rangle/L^2$ vs t/τ^0_{rod} for chains with $L=L_p$, where $\tau^0_{rod}\equiv\zeta_\perp L^3/(72k_BT)$ is the rod rotation time in dilute soluton. Numbers near curves are values of cL^3 (or "Dilute" for $c=0$), and numbers in parentheses indicate N. The black dashed line is the predicted asymptote at early times, for which $\langle \Delta d^2(t)\rangle \propto t^{3/4}$. Inset: $\langle \Delta \mathbf{r}^2_{m,\perp}(t)\rangle$ vs t/τ^0_{rod} for $L=L_p$ and cL^3= "Dilute," 100, 250, 500, 1000, and 2000. The red dashed line is the result of a slithering-snake simulation of pure reptation [16].

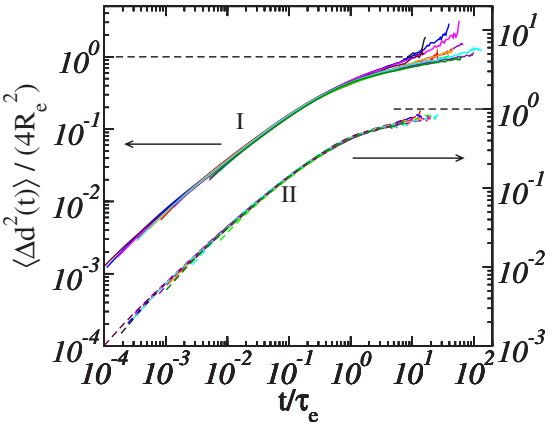

FIG. 2. (Color online) Collapse of $\langle \Delta d^2(t)\rangle$ data. Curves labeled "I" represent collapse of data for $N=20$, $cL^3=250,500,1000$, and $L/L_p=0.25,0.5,1.0,2.0$. Curves labeled "II" represent collapse of data for $N=40$, $cL^3=1000,2000,4000$, and $L/L_p=0.25,0.5,1.0,2.0$.

the tube (i.e., the average chain contour) in either of two transverse directions. A plateau would appear in $\langle \Delta d^2(t)\rangle$ even in the rigid-rod limit due to suppression of transverse center-of-mass motion. The suppression of $\langle \Delta \mathbf{r}^2_{m,\perp}(t)\rangle$ at intermediate times, however, is evidence of hindered *bending* motion, and thus of tight entanglement. In fact, we never observe a clean plateau in either quantity. Instead, we see a crossover from $t^{3/4}$ growth at small t to a much slower growth at intermediate times, which becomes flatter with increasing concentration (i.e., increasing cL^3), at a crossover time τ_e that decreases with increasing c. The suppression in $\langle \Delta \mathbf{r}^2_{m,\perp}(t)\rangle$ is significant only for $cL^3 \gtrsim 500$, suggesting a crossover concentration $c^{**}\simeq 500/L^3$ for $L=L_p$.

For $cL^3=1000$, our results for $\langle \Delta \mathbf{r}^2_{m,\perp}(t)\rangle$ include both a plateau at intermediate times and an upturn at the end of this plateau. The upturn is mimicked very accurately by the results of a separate slithering-snake simulation of pure reptation of a wormlike chain, shown by the dashed line in the inset (red online) [16]. Pure reptation yields a nonzero transverse MSD $\langle \Delta \mathbf{r}^2_{m,\perp}(t)\rangle$ at times less than the reptation time $\tau_{rep}=\zeta_\parallel L^3/(\pi^2 k_BT)$ because reptation occurs along a curved tube. $\langle \Delta d^2(t)\rangle$ is defined so as not to be affected by pure reptation, and so shows a broader plateau than $\langle \Delta \mathbf{r}^2_{m,\perp}(t)\rangle$.

To quantify τ_e and R_e, we have collapsed our data for $\langle \Delta d^2(t)\rangle$ in a manner that assumes the existence of a scaling relationship $\langle \Delta d^2(t)\rangle = 4R_e^2 f(t/\tau_e)$. That is, we have chosen values for R_e and an entanglement time τ_e for each set of parameters so as to collapse the data for many different values of L/L_p and cL^3 onto a master curve of $\langle \Delta d^2(t)\rangle/(4R_e^2)$ vs t/τ_e. The resulting collapse is shown in Fig. 2. We display separate master curves for chains with $N=20$ and $N=40$ because early-time behavior is noticeably different for chains with different numbers of rods. The collapse is excellent for solutions with $cL^3 \geq 1000$. The horizontal dashed lines with $\langle \Delta d^2(t)\rangle/4R_e^2=1$ represent an assumed long-time asymptote for hypothetical systems of much longer chains, from which we have extracted estimates of R_e.

Figure 3 shows resulting values of the dimensionless tube radius R_e/L_p vs dimensionless concentration ρL_p^2 for systems with $L/L_p=0.25$–2.0. Dimensional analysis requires that the

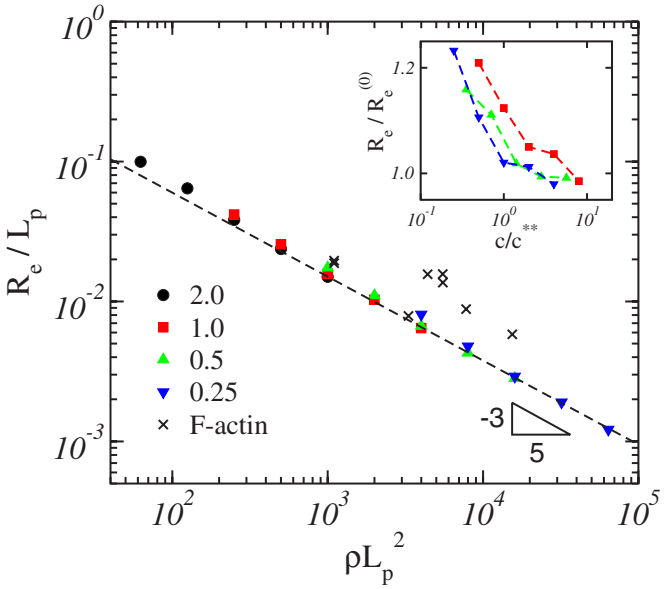

FIG. 3. (Color online) Nondimensionalized tube radius vs concentration. Numbers in the legend are values of L/L_p. Crosses are flourescence microscopy results for F-actin [8,9], nondimensionalized using $L_p=17$ μm. Inset: ratio $R_e/R_e^{(0)}$ vs c/c^{**}, where $R_e^{(0)}\equiv 0.95L_p(\rho L_p^2)^{-3/5}$ is the dashed line in the main plot and where $c^{**}=500L_p^{1/2}L^{-7/2}$.

ratio R_e/L_p be a function $R_e/L_p=f(\rho L_p^2, L/L_p)$ of dimensionless length L/L_p and dimensionless concentration ρL_p^2 alone. In the tightly entangled regime, however, we expect R_e to become independent of L, implying that R_e/L_p must approach a function of ρL_p^2 alone for $c \gg c^{**}$. At high concentrations, our results for different values of L/L_p do indeed approach a common asymptote, which is described extremely well by the predicted scaling relation $R_e/L_p = \alpha(\rho L_p^2)^{-3/5}$, with $\alpha=0.95$ (dashed black line). For each value of L/L_p, R_e/L_p also exhibits small but systematic deviations from this asymptote at lower concentrations. This deviation is emphasized in the inset, in which we plot the ratio $R_e/[0.95L_p(\rho L_p^2)^{-3/5}]$ vs c/c^{**}, where we have taken $c^{**}=500L_p^{1/2}L^{-7/2}$. The near collapse of the deviations from the asymptote for the stiffest two chains, $L/L_p=0.25$ and 0.5, confirms the prediction of a crossover $c^{**} \propto L_p^{1/2}L^{-7/2}$ for $L \ll L_p$ [5]. The experimental values for R_e in F-actin solutions (crosses) are flouresence microscopy results of Käs *et al.* [8,9], as analyzed and presented in Ref. [21].

The crossover from loose to tight entanglement is expected to cause a dramatic change in viscoelastic behavior. Detailed theories of linear viscoelasticity have been developed for the limits of dilute solutions ($c \ll c^*$) [17,18] and of very tightly entangled solutions ($c \gg c^{**}$) [6]. Both theories make use of a decomposition of the stress into curvature, orientational, and tension contributions [5] and of the dynamic modulus $G(t)$ (i.e., the response to an infinitesimal step strain) as a sum $G(t)=G_{\rm curv}(t)+G_{\rm ornt}(t)+G_{\rm tens}(t)$. In both dilute and loosely entangled solutions, $G_{\rm curv}(t)$ and $G_{\rm tens}(t)$ are predicted to exhibit power law decays at very early times, but to decay exponentially at times greater than the relaxation time $\tau_\perp=\beta\zeta_\perp L^4/(k_BTL_p)$ of the longest-wavelength bending mode, where $\beta=(4.74)^{-4}$. For all $c<c^{**}$, $G(t)$ is dominated at $t>\tau_\perp$ by a more slowly decaying orientational modulus of the form $G_{\rm ornt}(t) \simeq (3/5)ck_BTe^{-t/\tau_{rod}}$, where τ_{rod} is a rotational diffusion time. The plateau of magnitude $(3/5)ck_BT$ in $G_{\rm ornt}(t)$, which exists even in dilute solutions, reflects the entropy lost by partially aligning an initially random distribution of rod orientations. In loosely entangled solutions, entanglement is predicted to increase τ_{rod}, without changing this plateau modulus or significantly changing $G_{\rm curv}(t)$ or $G_{\rm tens}(t)$. The crossover to tight entanglement, however, is expected to cause a plateau to appear in $G_{\rm curv}(t)$, with a plateau value $G_{\rm curv,0}$ that varies as [4–7] $G_{\rm curv,0} \propto k_BT\rho^{7/5}L_p^{-1/5}$ for $c \gg c^{**}$.

We have "measured" $G(t)$ and its components by simulating stress relaxation after a rapid, small-amplitude uniaxial step extension of an initially cubic periodic unit cell. Stress is evaluated using the virial tensor, as in previous simulations of dilute solutions [17,18]. Measurements of $G(t)$ in dilute solution by this method agree to within statistical errors with those we obtained previously [17,18] from stress fluctuations in equilibrium.

In Fig. 4, the main plot shows a nondimensionalized sum $[G_{\rm ornt}(t)+G_{\rm curv}(t)]/(ck_BT)$ of the two components of $G(t)$ that are expected and observed to exhibit an elastic plateau. The inset shows $G_{\rm tens}(t)/(ck_BT)$, which, as expected [6], does not exhibit a plateau and which is found to be almost independent of c over this range of parameters. The plateau in

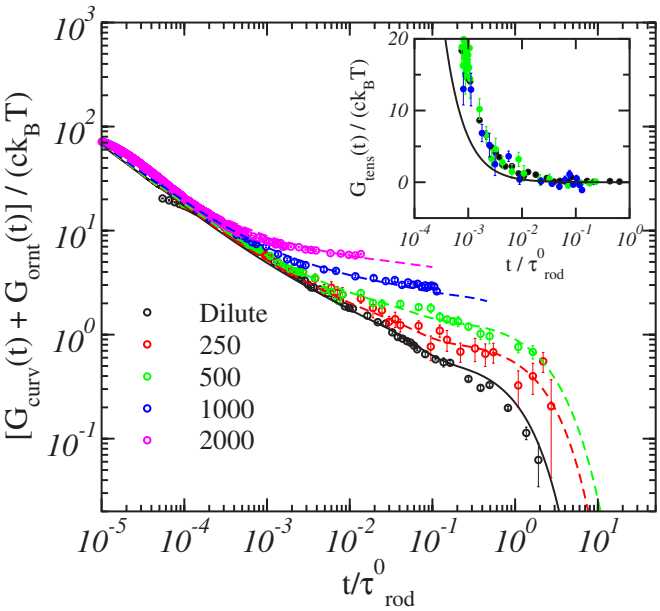

FIG. 4. (Color online) Nondimensionalized sum $[G_{\rm ornt}(t)+G_{\rm curv}(t)]/(ck_BT)$ vs t/τ^0_{rod} for $L/L_p=0.5$ and various values of cL^3 (shown in legend). Dashed curves are fits, as discussed in the text. Inset: corresponding tension stress $G_{\rm tens}(t)/(ck_BT)$ for systems with $cL^3=0$, 250, 500, 1000. Solid black curves in both plots are theoretical predictions for dilute solutions [18].

$[G_{\rm ornt}(t)+G_{\rm curv}(t)]/(ck_BT)$ becomes significantly greater than its dilute solution limiting value of 3/5, which arises from $G_{\rm ornt}(t)$ alone, only above an apparent crossover concentration of $c^{**}L^3 \sim 250$–500, above which $G_{\rm curv}(t)$ also contributes to the observed plateau. The terminal relaxation is accessible in our simulations only for $cL^3 \leq 500$, but the plateau value is always measurable.

To quantify the plateau modulus, we have fit the sum $G_{\rm curv}(t)+G_{\rm ornt}(t)$ to a function

$$\frac{3}{5}ck_BTe^{-t/\tau_{rod}} + G_{\rm curv,dil}(t) + G_{\rm curv,0}e^{-t/\tau_0}. \qquad (1)$$

Here, the first term on the right-hand side is an expression for $G_{\rm ornt}(t)$, where τ_{rod} is a concentration-dependent rotational diffusion time and $G_{\rm curv,dil}(t)$ is the prediction of Shankar *et al.* for $G_{\rm curv}(t)$ in dilute solution. The quantity $G_{\rm curv,0}$ is the contribution of $G_{\rm curv}(t)$ to the overall plateau modulus, which is an adjustable parameter. We have used a time constant $\tau_0=\tau_{rep}/2$ for the relaxation of the curvature plateau. This was chosen to fit the observed decay of $G_{\rm curv}(t)$ alone (not shown separately here) at $cL^3=250$ and 500, and is consistent with a double-reptation model for the relaxation of the curvature plateau. Values of the rotational diffusion time $\tau_{rod}(c)$ were measured in separate equilibrium simulations [15], which yield $\tau_{rod}/\tau^0_{rod}=(2.10, 3.06, 4.46, 6.17)$ for $cL^3=(250, 500, 1000, 2000)$. The values of $G_{\rm curv,0}$ obtained by fitting this data depend very little upon our choices for the time constants τ_0 and $\tau_{rod}(c)$.

The total plateau modulus G_0 in $G(t)$ is a sum $G_0=(3/5)ck_BT+G_{\rm curv,0}$ of orientational and curvature contribu-

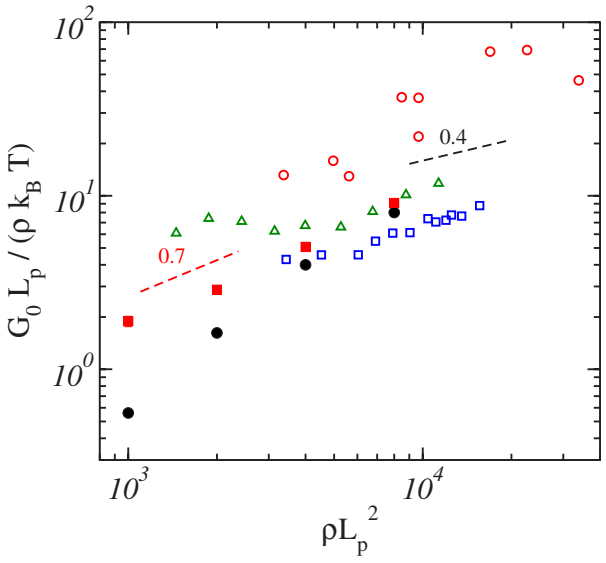

FIG. 5. (Color online) $G_0 L_p/(\rho k_B T)$ vs ρL_p^2 for both simulations and experiments on F-actin solutions. Simulation results are shown for G_0 (solid squares) and $G_{\mathrm{curv},0}$ (solid circles) for $L/L_p=0.5$. Results for F-actin solutions of Gardel *et al.* [12] (open circles) and of Hinner *et al.* [7] for filaments of unregulated length (open triangles) and of nominal average length 16 μm regulated by gelsolin (open squares). The dashed line with a slope of 0.4 is the scaling prediction $G_0 L_p/(\rho k_B T) \propto (\rho L_p^2)^{2/5}$, with the prefactor predicted by the binary collision approximation of Ref. [21].

tions. Figure 5 compares simulation results for G_0 and $G_{\mathrm{curv},0}$ to reported values of G_0 in entangled F-actin solutions [7,12]. The results of Hinner *et al.* [7] were obtained by macroscopic rheological measurements, while those of Gardel *et al.* [12] were obtained from two-particle microrheology. Our results for G_0 agree well with the values of Hinner *et al.* and are well within the scatter of results reported in the recent literature. A fit of our results for G_0 to a power of c yields $G_0/c \propto c^{0.7}$.

It is clear, however, that the range of concentrations accessed in our simulations, and most of that studied experimentally, lies within about one decade of the beginning of a broad crossover to tightly entangled behavior, below which $G_{\mathrm{curve},0}$ becomes negligible. As a result of this proximity to c^{**}, G_{ornt} dominates G_0 over much of this range, while the contribution $G_{\mathrm{curv},0}$, which is actually predicted to vary as $G_{\mathrm{curv},0}/c \propto c^{0.4}$ in the limit $c \gg c^{**}$, increases much more rapidly, from nearly zero. The results suggest that the rough agreement between the predicted behavior of $G_{\mathrm{curv},0}$ for $c \gg c^{**}$ and measurements of G_0 in F-actin is largely fortuitious.

The isotropic-nematic (IN) transition for rodlike polymers occurs at a concentration $c_{IN} L^3 \simeq 4L/d$ [13]. Values of L/d for available model systems with $L \lesssim L_p$ other than F-actin, such as Fd virus [22] ($L \simeq 0.9$ μm, $L_p \sim 2$ μm, $d \sim 7$ nm) and rodlike poly(benzyl glutatmate) [13] ($L_p \sim 0.15$ μm and $d \sim 2$ nm) are all at least 10 times smaller than for F-actin, for which $L/d \sim 10^3$. The IN transition in systems with $L/d < 100$ occurs at concentrations $c_{IN} L^3 \lesssim 400$, for which $c < c^{**}$. Our very rough estimate of $c^{**} \sim 500 L_p^{1/2} L^{-7/2}$ for $L \lesssim L_p$ suggests that a clearly defined tightly entangled isotropic regime for semiflexible rods should exist only in systems with $L/d \gtrsim 10^3$. This is consistent with the fact that a clear rheological signature of tight entanglement has been observed only in F-actin solutions.

Taken as a whole, our results both provide evidence for the correctness of a simple scaling theory for the asymptotic dependence of R_e vs c in tightly entangled solutions and clarify the limits of validity that theory, particularly as applied to rheology. It appears that bending fluctuations of rods with $L \sim L_p$ are significantly hindered by entanglement only under surprisingly stringent conditions.

This work has been supported by ACS Petroleum Research Fund Grant No. 38020-AC7, using computer resources of the Minnesota Supercomputer Center and of the UMN NSF MRSEC, under Award No. DMR-0212302.

[1] T. Odijk, Macromolecules **16**, 1340 (1983).
[2] M. Doi, J. Polym. Sci., Polym. Symp. **73**, 93 (1985).
[3] A. N. Semenov, J. Chem. Soc., Faraday Trans. 2 **82**, 317 (1986).
[4] H. Isambert and A. C. Maggs, Macromolecules **29**, 1036 (1996).
[5] D. C. Morse, Macromolecules **31**, 7030 (1998).
[6] D. C. Morse, Macromolecules **31**, 7044 (1998).
[7] B. Hinner, M. Tempel, E. Sackmann, K. Kroy, and E. Frey, Phys. Rev. Lett. **81**, 2614 (1998).
[8] J. Käs, H. Strey, and E. Sackmann, Nature (London) **368**, 226 (1994).
[9] J. Käs, H. Strey, J. X. Tang, D. Finger, R. Ezzell, E. Sackmann, and P. A. Janmey, Biophys. J. **70**, 609 (1996).
[10] M. Sato, G. Leimbach, W. H. Schwarz, and T. D. Pollard, J. Biol. Chem. **260**, 8585 (1985).
[11] F. G. Schmidt, B. Hinner, and E. Sackmann, Phys. Rev. E **61**, 5646 (2000).
[12] M. L. Gardel, M. T. Valentine, J. C. Crocker, A. R. Bausch, and D. A. Weitz, Phys. Rev. Lett. **91**, 158302 (2003).
[13] T. Sato and A. Teramoto, Adv. Polym. Sci. **126**, 85 (1996).
[14] M. Doi, J. Phys. (Paris) **36**, 607 (1975).
[15] S. Ramanathan, Ph.D. thesis, University of Minnesota, 2006.
[16] S. Ramanathan and D. C. Morse, J. Chem. Phys. **126**, 094906 (2007).
[17] M. Pasquali, V. Shankar, and D. C. Morse, Phys. Rev. E **64**, 020802(R) (2001).
[18] V. Shankar, M. Pasquali, and D. C. Morse, J. Rheol. **46**, 1111 (2002).
[19] A. Montesi, M. Pasquali, and D. C. Morse, J. Chem. Phys. **122**, 084903 (2005).
[20] R. Granek, J. Phys. II **7**, 1761 (1997).
[21] D. C. Morse, Phys. Rev. E **63**, 031502 (2001).
[22] F. G. Schmidt, B. Hinner, E. Sackmann, and J. X. Tang, Phys. Rev. E **62**, 5509 (2000).